



# Temporal and spatial scaling impacts on extreme precipitation

B. Eggert<sup>1</sup>, P. Berg<sup>2</sup>, J. O. Haerter<sup>3</sup>, D. Jacob<sup>1</sup>, and C. Moseley<sup>4</sup>

<sup>1</sup>Climate Service Center 2.0, Hamburg, Germany

<sup>2</sup>Hydrology Research unit, SMHI, Norrköping, Sweden

<sup>3</sup>Niels Bohr Institute, Copenhagen, Denmark

<sup>4</sup>Max Planck Institute for Meteorology, Hamburg, Germany

Correspondence to: B. Eggert (bastian.eggert@hzg.de)

Received: 1 December 2014 – Published in Atmos. Chem. Phys. Discuss.: 23 January 2015

Revised: 21 April 2015 – Accepted: 3 May 2015 – Published: 29 May 2015

**Abstract.** Convective and stratiform precipitation events have fundamentally different physical causes. Using a radar composite over Germany, this study separates these precipitation types and compares extremes at different spatial and temporal scales, ranging from 1 to 50 km and 5 min to 6 h, respectively. Four main objectives are addressed. First, we investigate extreme precipitation intensities for convective and stratiform precipitation events at different spatial and temporal resolutions to identify type-dependent space and time reduction factors and to analyze regional and seasonal differences over Germany. We find strong differences between the types, with up to 30 % higher reduction factors for convective compared to stratiform extremes, exceeding all other observed seasonal and regional differences within one type. Second, we investigate how the differences in reduction factors affect the contribution of each type to extreme events as a whole, again dependent on the scale and the threshold chosen. A clear shift occurs towards more convective extremes at higher resolution or higher percentiles. For horizontal resolutions of current climate model simulations, i.e.,  $\sim 10$  km, the temporal resolution of the data as well as the chosen threshold have profound influence on which type of extreme will be statistically dominant. Third, we compare the ratio of area to duration reduction factor for convective and stratiform events and find that convective events have lower effective advection velocities than stratiform events and are therefore more strongly affected by spatial than by temporal aggregation. Finally, we discuss the entire precipitation distribution regarding data aggregation and identify matching pairs of temporal and spatial resolutions where similar distributions are observed. The information is useful for planning observational

networks or storing model data at different temporal and spatial scales.

## 1 Introduction

The IPCC's fifth assessment report highlights an intensification of heavy precipitation events in North America and Europe (Hartmann et al., 2013) and projects further increase of extremes as global temperatures rise (Collins et al., 2013). The study of extreme events is complex due to a strong inhomogeneity of precipitation intensities in space and time. Assessment of precipitation extremes, e.g., as defined by an intensity threshold, is strongly scale dependent and therefore requires specification of the analyzed spatial and temporal resolution.

Even though spatial and temporal scales are far from independent (Taylor, 1938), it is often unclear how to compare data sets directly when their data are measured at differing resolutions. The data resolution needed by users, e.g., hydrologists or crop modelers, often differs from that at which observed or modeled data are recorded (Willems et al., 2012).

The primary societal interest in extreme precipitation lies in its hydrological implications, typically requiring statistics of precipitation extremes for the area of a given catchment or drainage system, which is not identical to that of model grid boxes or the observations.

Moreover, temporal scales relevant to flood risk vary enormously with area (Blöschl and Sivapalan, 1995; Westra et al., 2014): for catchments, hours to days are relevant (Mueller and Pfister, 2011), whereas urban drainage systems of  $\sim 10$  km (Arnbjerg-Nielsen et al., 2013) are impacted at

timescales from minutes to hours (De Toffol et al., 2009), and soil erosion can occur at even smaller scales (Mueller and Pfister, 2011).

Areal reduction factors (ARFs) and intensity–duration functions have previously been used to describe the decrease of average precipitation intensity due to spatial and temporal aggregation (Bacchi and Ranzi, 1996; Smith et al., 1994). The capability of radar data to capture the spatial structure of storms was identified as a key factor in deriving the ARFs (Bacchi and Ranzi, 1996; Arnbjerg-Nielsen et al., 2013). A general outcome was that ARFs exhibit a decay with respect to the return period (Bacchi and Ranzi, 1996; Sivapalan and Blöschl, 1998) and a dependency on the observed region, resulting from different governing rainfall generation mechanisms (Sivapalan and Blöschl, 1998).

In the current study we separate the physically different processes leading to convective and stratiform type precipitation events. Using synoptic observation data, we classify precipitation events into these two types, allowing us to analyze their aggregated statistics individually across scales.

The two types physically differ in that convection is often initiated by local radiative surface heating, resulting in a buoyantly unstable atmosphere (Houze, 1997), whereas stratiform precipitation stems from large-scale frontal systems and relatively weak and uniform up-lifting. Analyzing these two types separately regarding their intensities at different scales can, e.g., be important when considering temperature changes, such as anthropogenic warming: over large scales, the changes were found to be moderate, whereas for very small scales it has been argued that the two processes may increase with warming (Trenberth, 1999; Trenberth et al., 2003; Trenberth, 2011; Lenderink and van Meijgaard, 2008), albeit at very differing rates (Berg et al., 2013). Using high-resolution model simulations, heavy precipitation at high temporal resolutions was suggested to increase strongly in a future climate and a dominant contribution to extreme events to stem from convective events (Kendon et al., 2014; Muller et al., 2011; Attema et al., 2014). In spite of their small horizontal and temporal range, convective events can cause substantial damage (Kunz, 2007; Kunz et al., 2009), e.g., through flash floods (Marchi et al., 2010).

Numerous studies have assessed the temporal and spatial characteristics of precipitation events using a storm centered, or *Lagrangian*, approach (Austin and Houze Jr., 1972; Houze Jr. and Hobbs, 1982; Moseley et al., 2013) which focuses on the storm dynamics, e.g., lifetime or history of its spatial extent. Moseley et al. (2013) showed that, for Lagrangian event histories of 30 min, the convective type can produce significantly higher intensities than the stratiform type. As we here focus on potential hydrological applications and those addressing possible impact of extremes, e.g., floods, defining events over a *fixed* surface area and time period is more appropriate (Berndtsson and Niemczynowicz, 1988; Onof et al., 1996; Bacchi and Ranzi, 1996; Michele et al., 2001; Marani, 2003, 2005). The statistics thereby constitute aver-

ages over a defined space–time window within which both dry and wet sub-intervals may occur.

In this study, we analyze at which fixed temporal and spatial scales convective precipitation dominates precipitation extremes. To this end, we analyze 2 years of mid-latitude high-resolution radar data (5 min temporally and 1 km spatially), classified by precipitation types and separated into seasons (summer vs. winter) and geographic areas (northern vs. southern Germany). Analysis of these data over large spatial and temporal periods characterizes the statistical aggregation behavior in space and time. It can quantify the requirements on minimal model resolution sufficient for the proper description of the respective extremes. Revisiting the Taylor hypothesis (Taylor, 1938), we contrast the two precipitation types as to how resolutions in space and time can be compared. Using a resulting effective advection velocity, we give a simple means of quantifying effective temporal averaging in models, resulting from a given spatial resolution.

The structure of the article is as follows: in Sect. 2 we describe the data and methods used. Section 3 presents the results for extremes at different resolutions (Sect. 3.1) and suggests a method to compare the corresponding probability density functions (PDFs) (Sect. 3.2). We close with discussions and conclusions (Sect. 4).

## 2 Data and methods

A Germany-wide radar composite (RADOLAN-RY) from the German Weather Service is used in this study. This data set is provided on an approximate 900 km × 900 km grid with a 1 km horizontal resolution and contains information derived from 17 radar measurement facilities (Fig. 1). The rainfall rates ( $R$ ) were derived from raindrop reflectivities ( $Z$ ) using the  $Z$ – $R$  relationship (Steiner et al., 2004). The data are stored as discrete instantaneous intensities with an increasing bin size towards higher values. For the analysis, the 2-year time period covering 2007–2008 is considered. The data have been used (Moseley et al., 2013) and compared with gauge data previously (Berg et al., 2013).

For the current analysis, radar grid points are aggregated in time, i.e.,  $\Delta t \in \{5, 10, 15, 20, 30, 45, 60, 120, 180, 240, 360\}$  min, and in space over square grid box areas with linear dimensions  $\Delta x \in \{1, 2, 3, 4, 5, 6, 7, 8, 9, 10, 12, 15, 25, 50\}$  km. Aggregation includes all possible pairs  $\{\Delta t, \Delta x\}$ . Spatial aggregation is performed such that a coarser grid box starts at the bottom left corner of the domain and aggregates over the respective number of grid points towards the top right, with no overlap between the coarser grid boxes. As a consequence, the number of aggregated grid box scales  $\sim 1/(\Delta t \Delta x^2)$ . In cases where the original horizontal resolution cannot evenly be divided by the resolution of the coarser grid, the remaining grid points at the top and right border are not considered. This is the closest mimic of a gridded model.

Synoptic cloud observations, at 222 stations, obtained from the Met Office Integrated Data Archive System (MIDAS) data base ([http://badc.nerc.ac.uk/view/badc.nerc.ac.uk\\_\\_ATOM\\_\\_dataent\\_ukmo-midas](http://badc.nerc.ac.uk/view/badc.nerc.ac.uk__ATOM__dataent_ukmo-midas)) are used to separate large-scale and convective precipitation following Berg et al. (2013). The locations of the stations used are shown in Fig. 1. The classification process is carried out such that first a classification is made for each station and each 3 hourly observation into *convective*, *stratiform*, *mixed* or *no observations*. Second, to ensure more stable conditions, the classifications are aggregated in space to quadrants over the region (see Fig. 1) such that each quadrant contains one single classification for each 3 hourly time period. The aggregated classification can only be *convective* (*stratiform*) if there are no simultaneous observations of *stratiform* (*convective*) in the quadrant, or else the classification will be considered to be of the *mixed* type.

For the aggregated time resolutions 5 to 180 min, the precipitation is flagged as *convective*, respectively *stratiform*, according to the corresponding 3 hourly time slice. For time resolutions longer than 3 hours, two 3 hourly time slices have to be considered. Here we classify the precipitation event as *stratiform* or *convective* only if the type is identified at least at one of the time slices and the other time slice was not identified as the opposite type of event. This procedure was found to be the best compromise between rigid classification and sufficient data availability at the coarsest averaging windows.

Next, for each averaging window, the total number of convective and stratiform *events*, i.e., single time steps with an intensity higher than  $1 \text{ mm day}^{-1}$ , is counted. To ensure that enough events for statistical analysis are present, the analysis is restricted to resolutions where at least 500 convective and 500 stratiform events were detected. All other fields will be marked as insufficient (gray squares in the Figs. 3, 4 and 8).

### 3 Results

#### 3.1 Quantifying the impact of spatial and temporal aggregation on convective and stratiform precipitation extremes

##### 3.1.1 Differential impact on exceedance probabilities

We define the cumulative distribution function (CDF) as the probability of precipitation intensity exceeding a given intensity  $I$ :

$$\text{CDF}(\Delta t, \Delta x, I) \equiv \frac{\int_I^{\infty} N(\Delta t, \Delta x, I') dI'}{\int_{I_0}^{\infty} N(\Delta t, \Delta x, I') dI'}, \quad (1)$$

where  $N(\Delta t, \Delta x, I)$  is the number of data aggregates to resolution  $\Delta t$  and  $\Delta x$  with averaged precipitation intensity  $I$ , and  $I_0$  is the lower measurement cutoff. In the following, we

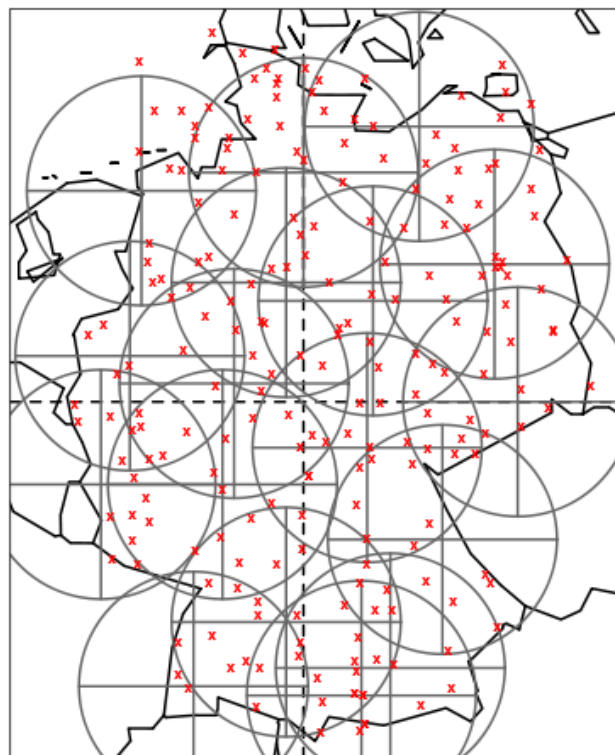


**Figure 1.** Data used in the analysis. Map of Germany with the synoptic stations (red crosses) and the radar locations and approximate range (gray circles). Dashed black lines indicate the division of the domain into quadrants.

choose  $I_0 = 1 \text{ mm day}^{-1}$  throughout.  $\text{CDF}(\Delta t, \Delta x, I)$  thus describes the percentiles of precipitation intensity when conditioning on wet periods. Figure 2 shows  $\text{CDF}(\Delta t, \Delta x, I)$  for Germany for different  $\Delta t$  and  $\Delta x$  conditional on convective and stratiform events. Note the logarithmic representation of the data, i.e., the figure focuses on the high precipitation intensities between the 99.9th percentile ( $10^{-1}$ ) and the 90th percentile ( $10^1$ ) of the distribution.

It is important to realize the effect of aggregation at varying scales. Consider first spatial aggregation (see legend in Fig. 2). Convection forms patterns with intense and localized precipitation peaks, separated spatially by regions without precipitation (Austin and Houze Jr., 1972; Moseley et al., 2013; Berg et al., 2013). Performing averages over areas of increasing size therefore yields broad variation of averages at small spatial scales but rapid decrease of variation as data are aggregated over larger areas. Stratiform precipitation is more uniform in the sense that sampling over small areas yields a good description of the statistics also at larger areas of aggregation.

Consider now temporal aggregation from an interval well below the convective lifetime (e.g.,  $\ll 30 \text{ min}$ ): the effect of temporal aggregation is to even out spatial variations due to the large-scale flow. This makes convection appear spatially

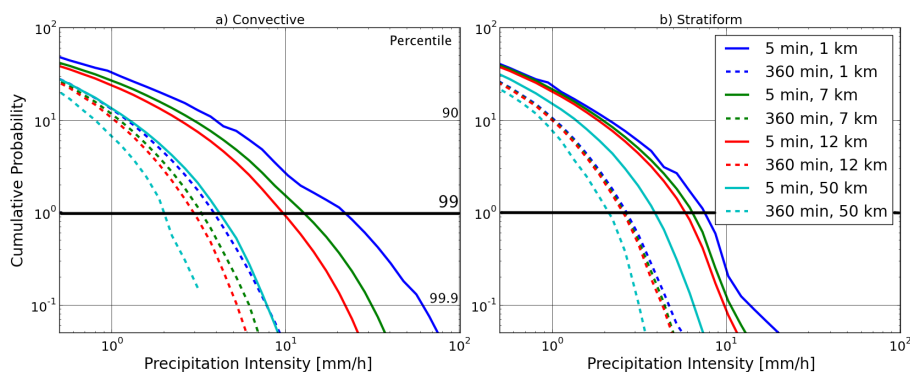


**Figure 2.** Cumulative probability density functions of precipitation intensities. All of Germany for the years 2007–2008, aggregated at different horizontal and temporal resolutions: (a) convective events and (b) stratiform events.

more uniform. For stratiform precipitation, patterns are already less localized in space and temporal aggregation will change the statistics less.

We make several observations in support of this assessment (Fig. 2): first, while convective precipitation can be much more intense (compare, e.g., the solid curves in Fig. 2a vs. b), the decrease of mean intensity due to aggregation is more pronounced than for stratiform precipitation. Second, we find that the relative differences in the CDFs between the 1 and 50 km data are stronger if the data are stored at 5 min resolution than for the 360 min data. For stratiform events we find almost no differences between precipitation intensities at resolutions below 12 km for a 360 min temporal resolution. Only at the largest regions, 50 km, do the spatial aggregations clearly modify the CDF as the non-precipitating region off the boundary of the event is included. This finding suggests that, for a given time resolution, there should be an associated horizontal resolution to store or collect data, i.e., a resolution that carries similar information about the distribution function.

More generally, this highlights the close match of the convective intensity CDFs when comparing two data sets of different resolution, namely 5 min and 50 km vs. 360 min and 1 km. For these pairs of resolutions time aggregation has a similar statistical effect on precipitation intensities as does spatial aggregation.

This latter observation can be appreciated when remembering the Taylor hypothesis of “frozen turbulence” (Taylor, 1938), which states that as the mean atmospheric flow advects eddies past a station, information about spatial variations can be gained as long as the properties of the eddies remain frozen in time. Consider, for example, an average convective event with constant precipitation intensity over its lifetime. According to Berg et al. (2013) and Moseley et al. (2013) the average convective event has a lifetime of approximately 30 min, a spatial extent of  $\sim 10$  km and a propagation speed of  $\sim 10$  m s $^{-1}$ . When using a 50 km grid box and 5 min temporal resolution, the event will move about 3 km;

therefore it can be assumed that the event stays in one grid box. It will affect roughly  $\frac{10 \times 10}{50 \times 50} \approx 4\%$  of the cell at a time. When an event of  $\sim 10$  km cross section moves over a location with  $\sim 10$  m s $^{-1}$ , its passage over the location would last  $\sim 1000$  s, which is  $\sim 17$  min and  $\frac{17}{360} \approx 5\%$  of the matching time interval of 6 h.

In the following we discuss how the actual observations depart from the approximation of the Taylor hypothesis and how this departure is influenced by the precipitation type. In reality, there are complications such that events change intensity also on short timescales, many events can be superimposed in space and time, and the large-scale flow is not constant.

To proceed, we now focus on intensity changes at a specific percentile, defined for a given combination of  $\Delta t$  and  $\Delta x$  by the inverse of Eq. (1), i.e., the intensity corresponding to a choice of exceedance probability. We will later return to the entire distribution functions in Sect. 3.2. Specifically, we now choose the 99th percentile of all detected precipitation events and refer to this percentile as *extreme precipitation*. This percentile was found to be a good compromise between the aim of focusing mainly on the high end of the intensity distributions and the need for sufficient data for the statistics. Using a percentile value as threshold to define precipitation extremes is a common practice.

For varying  $\Delta x$  and  $\Delta t$ , Figs. 3 and 4 show the 99th percentile of precipitation intensities for convective (termed  $\hat{I}_{cv}(\Delta t, \Delta x)$ ) and stratiform (termed  $\hat{I}_{ls}(\Delta t, \Delta x)$ ) events, respectively, for the entire region of Germany and separated into northern and southern Germany as well as for the whole year and separated into the summer (April–September) and winter (October–March) seasons. Note that we used a nonlinear scaling for the horizontal and vertical axes to better visualize the intensity changes at very high resolutions. The same plots as in Figs. 3 and 4 but with linear scales are shown in the Supplement. In the linear case the arcs, found when connecting fields with similarly extreme intensities, become almost straight lines. Straight lines mean that for any choice of

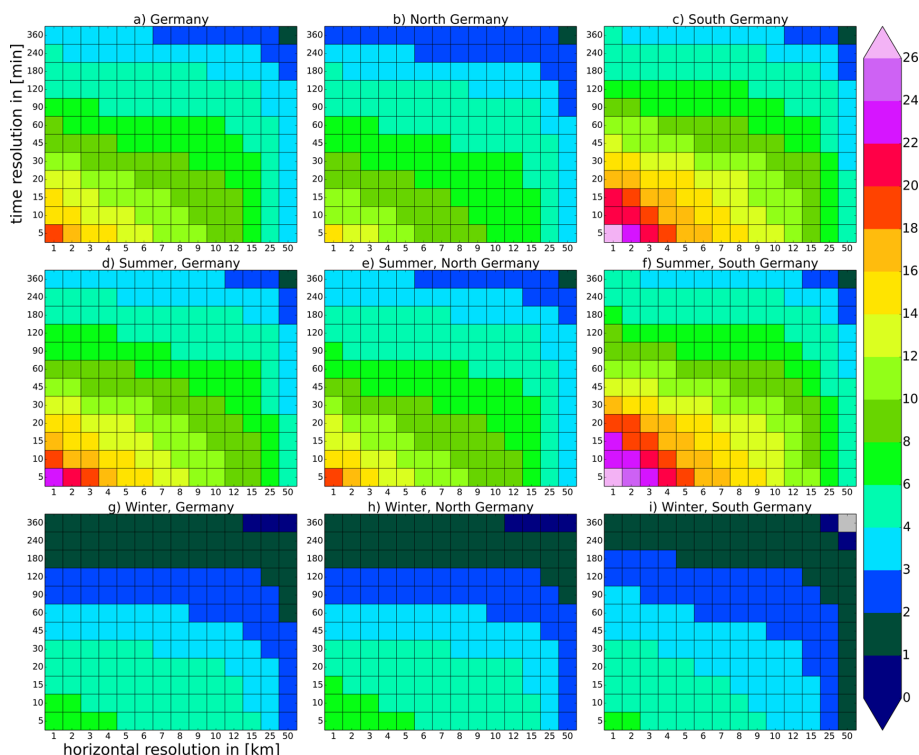


**Figure 3.** Convective extremes as a function of resolution. The 99th percentile of convective precipitation intensities, aggregated over different parts of Germany for the years 2007–2008, on different horizontal (horizontal axis) and temporal (vertical axis) resolutions: entire year (a–c), summer season (d–f) and winter season (g–i). All of Germany (a, d, g), northern Germany (b, e, h), southern Germany (c, f, i); intensities given in  $\text{mm h}^{-1}$ .

a resolution pair, equivalent resolutions, i.e., those of similar extremes, can be obtained by simple linear transformations.

When comparing  $\hat{I}_{\text{cv}}(\Delta t, \Delta x)$  (Fig. 3) to  $\hat{I}_{\text{st}}(\Delta t, \Delta x)$  (Fig. 4), it is striking that at high temporal and spatial resolutions the intensity  $\hat{I}_{\text{st}}$  is only about one-third of  $\hat{I}_{\text{cv}}$ . However,  $\hat{I}_{\text{st}}$  shows much less spatial and seasonal differences when compared to  $\hat{I}_{\text{cv}}$ . For example, the increase in intensity at the highest resolution in summer vs. winter is about 220 % for  $\hat{I}_{\text{cv}}$  but only approximately 20 % for  $\hat{I}_{\text{st}}$ . This finding is in line with the relatively weak temperature response of stratiform precipitation intensities as reported recently (Berg et al., 2013).

Regionally, southern Germany exhibits higher  $\hat{I}_{\text{cv}}$  in summer as compared to the north. This may largely be due to not only complex orographic areas in southern Germany, e.g., the highly convectively active area of the Black Forest in southwestern Germany (Khodayar et al., 2013), but also latitudinal temperature differences and the more continental climate of the south.

The highest intensities of stratiform precipitation occur in northern Germany in the months May to September. We find that for time durations shorter than 3 h the highest intensities occur between June to August. For longer time durations, the highest intensities occur in the months September to November (see Supplement).

### 3.1.2 Scaling behavior of convective and stratiform precipitation events

To quantify the reduction due to spatial aggregation, we define the area reduction factor  $\text{ARF}(\Delta x)$  as the reduction of the 99th percentile at spatial resolution  $x$  relative to the percentile (here defined as  $\hat{I}_{\text{ori}}$ ) at the original resolution (5 min, 1 km). Varying now the spatial resolution while keeping the temporal resolution fixed (at 5 min), we define

$$\text{ARF}(\Delta x) \equiv 1 - \frac{\hat{I}(\Delta x)}{\hat{I}_{\text{ori}}}, \quad (2)$$

where  $\hat{I}$  and  $\hat{I}_{\text{ori}}$  is shorthand for either of the precipitation types. Analogously, we define the duration reduction factor  $\text{DRF}(\Delta t)$  as the intensity reduction due to temporal aggregation relative to  $\hat{I}_{\text{ori}}$ , while keeping the spatial resolution at 1 km, i.e.,

$$\text{DRF}(\Delta t) \equiv 1 - \frac{\hat{I}(\Delta t)}{\hat{I}_{\text{ori}}}. \quad (3)$$

ARFs and DRFs are shown in Fig. 5a and b, respectively, for both precipitation types and separately for the summer and winter seasons, as well as for northern and southern Germany. Considering  $\hat{I}_{\text{cv}}$ , a strong intensity reduction can be

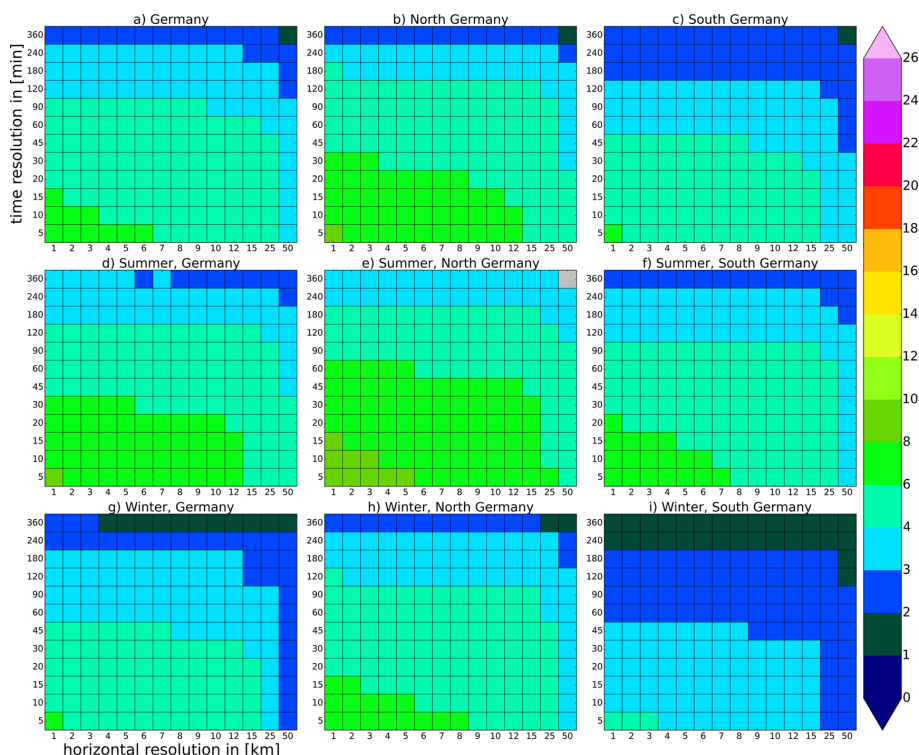


**Figure 4.** Stratiform extremes as a function of resolution; otherwise similar to Fig. 3.

seen when the spatial (Fig. 5a) or temporal (Fig. 5b) resolution is decreased. The reduction due to spatial aggregation shows clear seasonal and regional differences: the lowest ARFs occur in northern Germany in winter (68 % at 50 km grid size) and the highest in southern Germany in summer (84 % at 50 km grid size). Temporal aggregation is nearly independent of seasonal and regional distinctions and reaches values of about 80 to 85 % at a 6 hourly resolution. The differences found between  $\hat{I}_{cv}$  and  $\hat{I}_{ls}$  are hence larger than all other seasonal or regional differences within one type.

$\hat{I}_{ls}$  shows much less pronounced ARFs and DRFs. For the maximum spatial aggregation, only 52 % reduction is found in northern Germany in winter. The seasonal and regional differences are smaller than for  $\hat{I}_{cv}$  and differ only by less than 10 percentage units. Temporal aggregation shows also only small regional and seasonal differences, causing DRFs of 60 to 70 % at a temporal resolution of 6 h.

### 3.1.3 Comparing the relevance of space compared to time aggregation

We can distinguish the behavior of spatial and temporal aggregation using two kinds of approaches (Deidda, 2000). The first approach would be to regard precipitation as a self-similar process (simple scaling). In this case the Taylor hypothesis (Taylor, 1938) would be obeyed, and temporal variations can be reinterpreted as spatial variations that are ad-

ducted over a fixed location by a large-scale flow that is constant over the observed temporal and spatial scales.

Following the notion of “frozen turbulence”, intensity change due to spatial aggregation can then be calculated from the intensity changes that result due to temporal aggregation multiplied by a constant velocity  $u$ , i.e.,  $\Delta x \approx \Delta t \cdot u$ . This would only hold if precipitation extremes could be seen as objects of temporally constant characteristics that are translated by large-scale advection. If we also assume spatial inhomogeneity only to occur in the advection direction, a gauge station could be used to measure the precipitation intensities that fall over an area (Fig. 6a).

The second approach would assume that the spatial and temporal aggregation behavior of precipitation extremes would behave like a self-affine process (a process where the ratio of scales is changing as one of the scales changes). In this case, the simple linear relation that connects changes due to time aggregation with changes due to spatial aggregation through an advection velocity generally does not hold anymore (e.g., due to temporal (Fig. 6b) or spatial inhomogeneity (Fig. 6c)). A multifractal analysis is needed where, in short, the “velocity” itself would become a function of the respective spatial and temporal scales. If this function is known, it is possible also for self-affine processes to connect spatial and temporal scales. Proper understanding of the relationship between spatial and temporal aggregation is crucial,

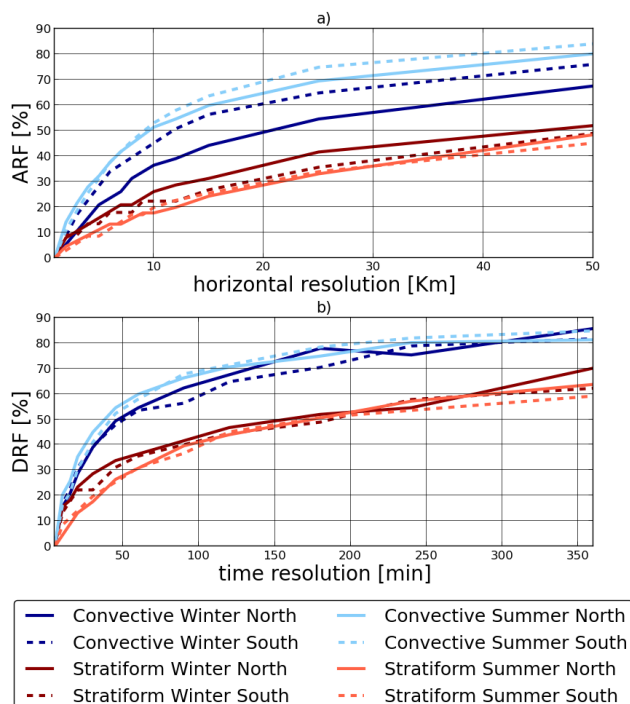


**Figure 5.** Area and duration reduction factors. **(a)** Area reduction factors at 5 min temporal resolution. **(b)** Duration reduction factors (DRFs) for 1 km × 1 km spatial resolution in percent for convective (blue) and stratiform (red) precipitation. Data shown for the summer and winter seasons and northern and southern Germany.

e.g., for precipitation downscaling and bias correction methods (Wood et al., 2004; Piani et al., 2010a, b).

Our goal here is to characterize the differences in scaling of convective and stratiform extremes. Comparing the intensity reduction due to time aggregation for the 1 km data set (Fig. 3a, left column) with the intensity reduction that results from spatial aggregation at a temporal resolution of 5 min (bottom row), a 4 km spatial aggregation is comparable to that of spatial aggregation for roughly 15 min. Similarly, for stratiform precipitation (Fig. 4a) we find that 6 km spatial aggregation corresponds to 15 min temporally. There is hence a dependence on the precipitation type, a relation we now analyze.

Figure 7a shows for each horizontal resolution the matching temporal resolution that achieves similar intensity reduction. We describe the relation between temporal and spatial aggregation at a fixed  $\Delta x$  by

$$f_{\Delta x}(\Delta t) = |\hat{I}(\Delta t, 1 \text{ km}) - \hat{I}(5 \text{ min}, \Delta x)|. \quad (4)$$

We now define  $\phi_{\Delta x}$  as the minimum value of  $f_{\Delta x}$  w.r.t.  $\Delta t$ :

$$\phi_{\Delta x} = \min_{\Delta t} f_{\Delta x}(\Delta t). \quad (5)$$

The best matching time window  $\Delta t$  for a given  $\Delta x$  can be determined using the inverse function of  $f_{\Delta x}$ :  $\Delta t = f^{-1}(\phi)$ .

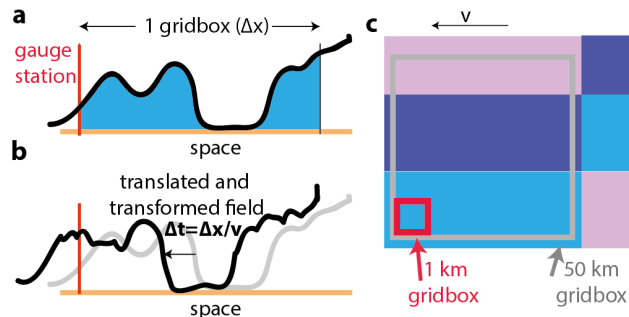


**Figure 6.** Schematic illustration of the Taylor hypothesis. **(a)** One-dimensional case showing space, grid box width and precipitation intensity (black curve); the location of a gauge station is marked in red. **(b)** Similar to **(a)** but illustrating how the curve may change due to small-scale dynamics after a time interval  $\Delta t = \Delta x/v$ , with  $v$  the atmospheric advection velocity. **(c)** Two-dimensional inhomogeneities (different colors indicate different intensities) perpendicular to the advection direction (direction indicated by the thin arrow). Small (red) and large (gray) grid boxes as marked.

In practice, we determine  $\Delta t$  by an iterative numerical procedure, using first an interpolation between available resolutions for better approximation. The result for several high percentiles is shown for both precipitation types over Germany for the entire year on a log–log plot (Fig. 7a), i.e., straight lines represented power laws. If the Taylor hypothesis is obeyed, the exponent would equal unity.

Within the limitations of the relatively noisy data, we find that the data represent a straight line over most of the analyzed spatial range and can be fitted to a power law function  $\Delta t = a \times \Delta x^b$  with fitting parameters  $a$  and  $b$ , or by using dimensionless variables (i.e., defining  $\chi \equiv \Delta x/\Delta x_0$ ,  $\tau \equiv \Delta t/\Delta t_0$  and  $\tilde{a} \equiv a \Delta x_0^b/\Delta t_0$ ) we have

$$\tau = \tilde{a} \chi^b, \quad (6)$$

with fitting parameters  $\tilde{a}$  and  $b$ . The parameter  $\tilde{a}$  is a scaling parameter and describes the  $\Delta t_0$  corresponding to  $\Delta x_0$ .  $\chi^b$  describes how the relevance of space compared to the time aggregation changes with resolution.

In Fig. 7a and b, the best fit for the 99th intensity percentile is shown for convective and stratiform precipitation. We find that  $b$  is similar for both types (generally between 1.17 and 1.32), a departure from unity that should be confirmed by other data sources than the radar data at hand. An exponent  $b > 1$  indicates that extreme precipitation is self-affine (self-similarity would require  $b = 1$ ). The fractal properties of precipitation were already highlighted in earlier studies and are found to be a result of the hierarchical structure of precipitation fields (Schertzer and Lovejoy, 1987) with cells that are embedded in small mesoscale areas which in turn occur in clusters in large-scale synoptic areas (Austin and Houze Jr., 1972).

Table 1 displays  $\tilde{a}$  and  $b$  for the different percentiles shown in Fig. 7a (non-dimensional). We find that for convective pre-

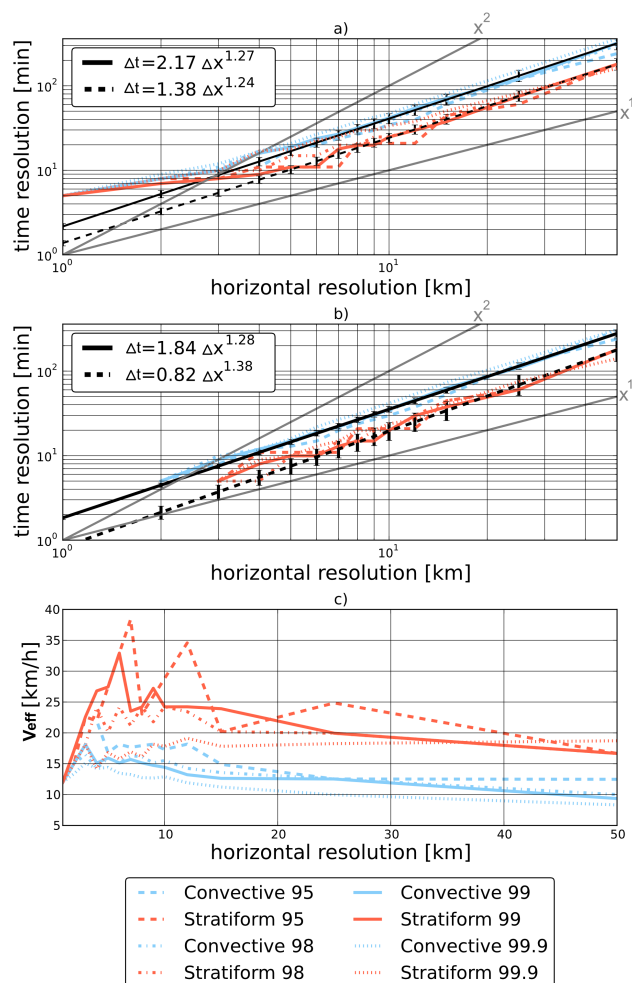


**Figure 7.** Consistent spatial and temporal resolutions.  $\Delta t$  derived using Eq. (5) for different values of  $\Delta x$  for convective (blue) and stratiform (red) precipitation extremes at the 95th, 98th, 99th and 99.9th percentiles. Black lines are least square fit of  $\Delta t = a \times \Delta x^b$  with the fitting parameters  $a$  and  $b$  for the 99th percentile. Error bars indicate the standard deviation of parameter estimates. Gray lines show  $\Delta t \sim \Delta x$  and  $\Delta t \sim \Delta x^2$ . (a) Initial resolutions  $\Delta t_0 = 5$  min,  $\Delta x_0 = 1$  km. (b)  $\Delta t_0 = 5$  min and aggregated spatial resolutions  $\Delta x_0 = 2$  km (convective) and  $\Delta x_0 = 3$  km (stratiform). (c)  $v_{\text{eff}}$  (Eq. 7) for both precipitation types for Germany over the entire year.

precipitation  $\tilde{a}$  is near 0.5. Within the error bars there is no obvious dependence on percentile. This is also the case for the stratiform type but not for the 99.9th percentile, which has higher  $\tilde{a}$  and lower  $b$  values.

Since the values of  $b$  are similar for both precipitation types (Table 1), the difference between the matching temporal resolution of stratiform and convective events is kept constant over the entire range of  $\Delta x$  analyzed. We find that the different scaling between the two precipitation types mainly results from the varying  $\tilde{a}$ .

**Table 1.** Estimation of the exponent  $b$  and the pre-factor  $\tilde{a}$  for the different precipitation types and percentiles together with the standard deviation of the parameter estimate.

Precipitation type	Percentile	$\tilde{a}$	$b$
Convective	95th	$0.51 \pm 0.05$	$1.17 \pm 0.03$
	98th	$0.45 \pm 0.03$	$1.25 \pm 0.02$
	99th	$0.43 \pm 0.04$	$1.27 \pm 0.02$
	99.9th	$0.55 \pm 0.01$	$1.24 \pm 0.01$
	mean	$0.49 \pm 0.03$	$1.23 \pm 0.02$
Stratiform	95th	$0.20 \pm 0.04$	$1.32 \pm 0.06$
	98th	$0.35 \pm 0.03$	$1.18 \pm 0.02$
	99th	$0.28 \pm 0.02$	$1.24 \pm 0.02$
	99.9th	$0.76 \pm 0.03$	$0.96 \pm 0.01$
	mean*	$0.28 \pm 0.03$	$1.25 \pm 0.03$

\* Excluding the 99.9th percentile.

Note also the kink in the observed curves in Fig. 7a at about 6 km, where a change of slope is observed. To show that this kink is a manifestation of the scale mismatch, we aggregate data spatially to 2 km (3 km for stratiform) horizontal resolution and re-plot (Fig. 7b). Due to this procedure the kink almost vanished. This test shows that aligning resolutions according to Eq. (6) allows smooth scaling.

For further analysis, and to make contact to the Taylor hypothesis, we use the ratio of the matching  $\Delta x$  and  $\Delta t$  to calculate the mean *effective* advection velocity, which we call  $v_{\text{eff}}$ . We define

$$v_{\text{eff}}(\chi) \equiv \chi/\tau = \chi^{1-b}/\tilde{a}. \quad (7)$$

This effective velocity is not obviously the same as the velocity obtained by tracking algorithms, such as in Moseley et al. (2013), as  $v_{\text{eff}}$  combines all reasons for changes caused by aggregation. The main sources for these changes are advection of the precipitation field out of the grid box, temporal inhomogeneity caused by the temporal evolution of the precipitation event (Fig. 6b) and horizontal inhomogeneities perpendicular to the advection direction, which will increase the area reduction factors (Fig. 6c).

Figure 7c shows  $v_{\text{eff}}$  calculated for different  $\Delta x$  for the 95th, 98th, 99th and 99.9th percentile, using data without seasonal distinctions over Germany.  $v_{\text{eff}}$  lies in the same range as the velocities calculated by Deidda (2000) and Moseley et al. (2013) who calculated the velocities using tracking techniques. This shows that advection is likely the major source for changes due to temporal and horizontal aggregation. Low  $v_{\text{eff}}$  for horizontal resolutions below about 2 to 4 km are again a result of the mismatch of the 5 min temporal resolution and the 1 km spatial resolution explained above.

Note the deviating value of  $\tilde{a}$  for the 99.9th percentile of stratiform precipitation. This could be explained by mesoscale stratiform systems with embedded convection,

i.e., systems that are somewhat intermediate between stratiform and convective events. The corresponding graph (Fig. 7c) shows intermediary behavior, connecting the curves of convective precipitation (low  $\Delta x$ ) to those of stratiform precipitation at high  $\Delta x$ . Due to substantial noise at high spatial resolution it is not possible to identify whether  $v_{\text{eff}}$  shows a constant behavior ( $b = 1$ ) at the high resolutions, therefore the results in Zawadzki (1973) and Waymire et al. (1984) that indicate the Taylor hypothesis holds for timescales less than 40 min can neither be confirmed nor rejected.

Realizing that  $v_{\text{eff}}$  combines all sources for changes caused by aggregation enables a simplified view on the aggregation process. In a similar way as in Deidda (2000) we can use  $v_{\text{eff}}$  to generalize the Taylor hypothesis for a self-affine process by using  $v_{\text{eff}}$  instead of a constant velocity to describe the relation between space and time. Following the Taylor hypothesis we can now interpret the matching temporal and spatial scales from Fig. 7a as the mean time that is needed to advect the information about the precipitation field over the matching horizontal scale (implicitly including all other sources of aggregation changes as described above). For example the typical timescale for a convective precipitation area to cross a grid box with a 10 km grid size, a typical resolution of state-of-the-art climate models, would be about 40 min. For a stratiform precipitation event the information about the precipitation field is already captured after about 20 to 25 min. Reasons for the lower effective advection velocity might be that stratiform events are statistically more homogeneous than convective events which results in a shorter period to capture the structure of the event. Also, convective events often occur at high-pressure weather conditions where low wind velocities might entail lower advection velocities.

Aggregation effects at a specific resolution will always be a combination of duration and area reduction factors. Connecting space and timescales using  $v_{\text{eff}}$  allows the association of temporal and spatial scales, shown in Fig. 7a. If, for a given spatial resolution, a larger temporal output period is used as indicated by Fig. 7a, the event will on average be advected beyond the grid box area, leading to high duration reduction factors (a “smearing out”).

### 3.1.4 Dominance of convective vs. stratiform extremes including event occurrences

So far we have only illustrated differences in the 99th percentiles of detected convective and stratiform events with precipitation intensities above  $1 \text{ mm day}^{-1}$ , i.e., conditional probability density functions. The sample size therefore depends on the number of detections of the specific precipitation type, the resolution of the data set and the area fraction in the detected quadrants with precipitation intensities higher than the specified threshold. Including the events without precipitation in the statistics will have a major impact on the percentile values; therefore a sensitivity analysis per-

**Table 2.** Occurrence of convective and stratiform events. Number of quadrants of Germany classified as convective (C) or stratiform (S) in the 3 hourly synoptic observations. The maximum possible values for the 2 years and for all four quadrants is 23 360. This number reduces by about half for the seasonal data and again by half for the sub-regions of Germany.

Area	Type	Year	Summer	Winter
All	S	1358	206	1152
All	C	1537	1270	267
North	S	761	103	658
North	C	741	590	151
South	S	597	103	494
South	C	796	680	116

forming the same analyses shown in Figs. 3 and 4 but with non-conditional probability density functions was done (not shown). This demonstrated that  $v_{\text{eff}}$  is not strongly affected by this threshold. Naturally, due to the high number of non-precipitation values, the high percentiles show correspondingly lower intensities. Table 2 indicates the event occurrences classified as convective or stratiform in the 3 hourly synoptic observations.

To consider the strong variation in occurrences, e.g., concerning season, we find that also the relative occurrence frequency of the two types of events has to be accounted for. We again use the 99th percentile for all data above  $1 \text{ mm day}^{-1}$ , but now without distinction of precipitation type, for each aggregation interval as well as for each region and season. In the following we redefine  $\hat{I}$  as the corresponding intensity (see Supplement for  $\hat{I}$  values).

To assess the relative likelihood of a certain precipitation type to cause extreme precipitation, Fig. 8 shows the ratio of the number of convective events exceeding the intensity  $\hat{I}$  vs. the total number (convective + stratiform) of events exceeding  $\hat{I}$ , i.e.,  $N_{\text{cv}}(I > \hat{I}) / (N_{\text{cv}}(I > \hat{I}) + N_{\text{ls}}(I > \hat{I}))$ .

However, dominance again depends on resolution: e.g., in southern Germany (all year) 80–90 % of precipitation extremes are of the convective type for the higher resolutions. Only when the data are aggregated to resolutions with grid spacings of 25 km and more does the percentage of stratiform events become appreciable. Even stronger differences occur between seasons: in summer, convection dominates extremes but is of less importance in winter (less than 10 % for the aggregated data sets and less than 35 % even at the very high-resolution data sets).

It is important to note that we used a percentile threshold for this analysis and the corresponding intensity threshold fluctuates with seasons. To test whether our findings simply are a consequence of overall higher intensities in summer we also compare similar intensities for summer and winter (using the 98th percentile for summer and the 99th percentile in winter, see Fig. 8g–i and Supplement). This revealed that seasonal differences nonetheless prevail.

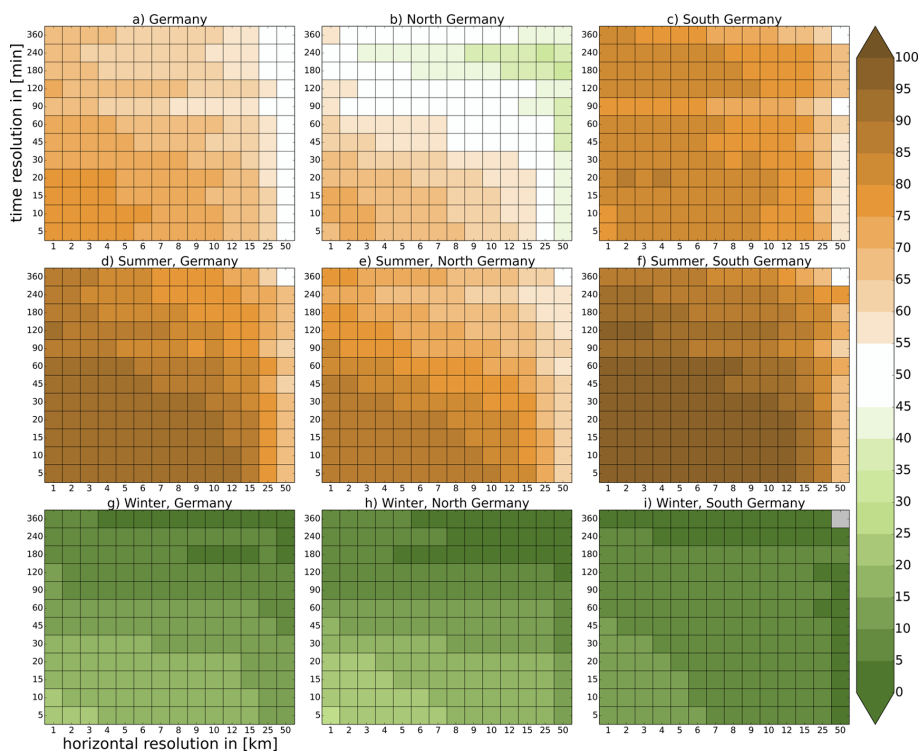


**Figure 8.** Convective dominance as a function of resolution including dry periods. The ratio of the number of convective precipitation events with precipitation intensities greater than or equal to the threshold intensity. Threshold intensity is defined as the 99th percentile of total precipitation intensities over the different parts of Germany for the years 2007–2008. Panels otherwise as in Fig. 3.

Figure 9 shows the convective dominance as a function of the horizontal resolution for the 95th, 98th, 99th and 99.9th percentiles. The role of convective precipitation in the extremes increases with higher percentiles, and convective precipitation becomes more relevant also over larger aggregated areas and time steps (see Supplement). At relatively low percentiles convective and stratiform events have the same exceedance probability, but with increasing percentile convection dominates, especially at high spatial resolution.

### 3.2 Assessing PDF changes due to data aggregation

The results of Sect. 3.1 highlight the interdependence of spatial and temporal scales and their impact on extreme precipitation. Changing resolutions, however, modifies the entire distribution function. To give an estimate of the information loss due to the aggregation process, we adopt a measure similar to that of the Perkins skill score (Perkins et al., 2007), originally designed to validate a model against observations by assigning a skill score. Here, we use it to quantify the overlap between two intensity PDFs at different horizontal and temporal resolutions. We define the *PDF overlap* as

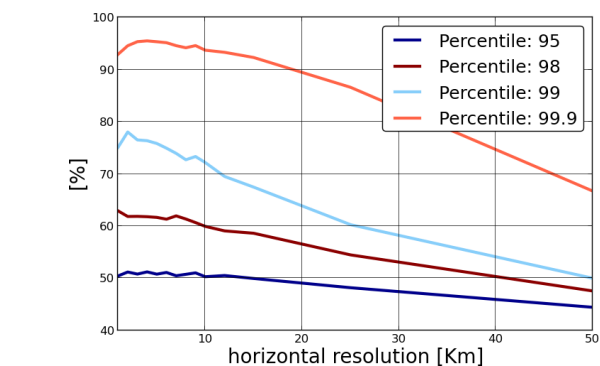


**Figure 9.** Convective dominance vs. horizontal resolution. The ratio of the number of convective precipitation events with precipitation intensities greater than or equal to the labeled percentile of total precipitation intensities over entire Germany for the years 2007–2008. The data are aggregated to 5 min temporal and different horizontal resolutions.

$$S(\Delta t_1, \Delta x_1; \Delta t_2, \Delta x_2) \equiv \int_{I_0}^{\infty} \min(\rho_{\Delta t_1, \Delta x_1}(I), \rho_{\Delta t_2, \Delta x_2}(I)) dI, \quad (8)$$

where  $I$  is precipitation intensity,  $I_0$  is the measurement cutoff,  $\rho_{\Delta t, \Delta x}(I)$  is the normalized PDF as in Eq. (1) and  $\min(\cdot, \cdot)$  gives the minimum of the two arguments. Hence,

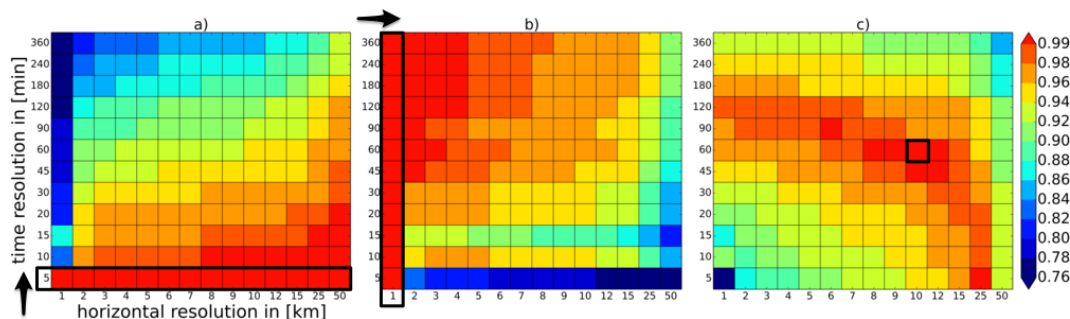


**Figure 10.** PDF overlap for convective precipitation intensity. All of Germany for the years 2007–2008, aggregated to different horizontal (horizontal axis) and temporal (vertical axis) resolutions. **(a)** PDF overlap of each horizontal resolution between every temporal resolution and the 5 min data. **(b)** PDF overlap of each temporal resolution between every horizontal resolution and the 1 km data. **(c)** PDF overlap of each horizontal and temporal resolution compared to the 10 km, 60 min data.

$S(\Delta t_1, \Delta x_1; \Delta t_2, \Delta x_2)$  quantifies the overlap between PDFs of aggregated data at the spatiotemporal resolutions  $(\Delta t_1, \Delta x_1)$  and  $(\Delta t_2, \Delta x_2)$ . If the two PDFs are identical, the overlap value is 1; if there is no overlap at all, it is 0. The PDF overlap is a means of comparing not only a fixed percentile of precipitation intensity but measuring the similarity of entire distribution functions. It is hence a way to quantify our initially qualitative discussion regarding Fig. 2.

We aggregate convective precipitation intensities over Germany and present the PDF overlap in three different ways: Fig. 10a shows the PDF overlap between the aggregated time resolution with the corresponding 5 min data but at fixed horizontal resolution, i.e.,  $S(5 \text{ min}, \Delta x; \Delta t, \Delta x)$  at matrix element position  $(\Delta t, \Delta x)$ . For the spatially highly resolved data ( $\Delta x < 7 \text{ km}$ ), the PDF overlap degrades quickly when temporal resolution is reduced, while degradation is much slower at lower spatial resolution. In practice, if a defined spatial area, say a metropolitan region of 25 km, is of interest, performing measurements at 60 min resolution may lead to a tolerable margin of error while a smaller region of 2 km would require 5 or 10 min temporal resolution for the same margin of error. The chart could hence be used to estimate the error when data are available at one resolution but another is of interest. In Fig. 10b we present an analogous analysis, but we have now fixed the temporal resolution and compare to the 1 km data sets, i.e.,  $S(\Delta t, 1 \text{ km}; \Delta t, \Delta x)$  at matrix element position  $(\Delta t, \Delta x)$ . A similar pattern emerges with degradation now occurring for decreased spatial resolution.

In a third analysis (Fig. 10c) we calculate the overlap  $S(60 \text{ min}, 10 \text{ km}; \Delta t, \Delta x)$  among aggregated data of spatiotemporal resolution  $(t, x)$  and the data set at 60 min temporal resolution and 10 km spatial resolution. This reference point was chosen because it is close to current state-of-the-art regional climate model simulation over Europe. The plot shows a ridge with values close to 1, ranging from 5 min and 25 km to 120 min and 1 km resolution. Apparently all spatiotemporal resolutions along this curve produce PDFs which

differ only slightly from the 5 min, 10 km aggregation. PDF overlap values quickly decrease when departing from this ridge. Comparing this ridge with the intensity decrease in the 99th percentile as illustrated in Fig. 3a, we find that the PDF overlap mirrors the changes found in the 99th percentile. Using cumulative PDF measures as the Kolmogorov–Smirnov statistics is an alternative way of comparing PDFs. Figure 10c shows that different pairs of resolution give very similar PDFs. This can be used when comparing data sets of different resolution. This information also proved to be useful for statistical bias correction, further analyzed in the paper by Haerter et al. (2015).

For stratiform precipitation (Fig. 11), the analogous PDF overlap degrades more slowly compared to convective precipitation. For example, at a 50 km grid size we find that twice the temporal aggregation can be tolerated as compared to convective precipitation when a given PDF overlap is demanded (Fig. 11a). Similar conclusions hold for the degradation as function of horizontal resolution (Fig. 11b). Starting at about 20 min we again find that the  $\Delta x$  can be increased to about twice the value for convective events to achieve the same PDF overlap value. For the overlap  $S(60 \text{ min}, 10 \text{ km}; \Delta t, \Delta x)$ , shown in Fig. 11c, the lower sensitivity to resolution changes for stratiform precipitation translates to a substantial widening of the red-shaded area near the ridge, indicating much lower errors of estimating extremes at unavailable resolutions when stratiform precipitation is concerned compared to the case for convective precipitation (Fig. 10c). Performing measurements over extended regions can already serve as a reasonable predictor of more local extremes. We also find that due to the different area and duration reduction factors of stratiform and convective type events, the ridge with values close to 1 is shifting. For the stratiform type we find that this ridge ranges from 5 min and 25 km to 90 min and 1 km resolution.

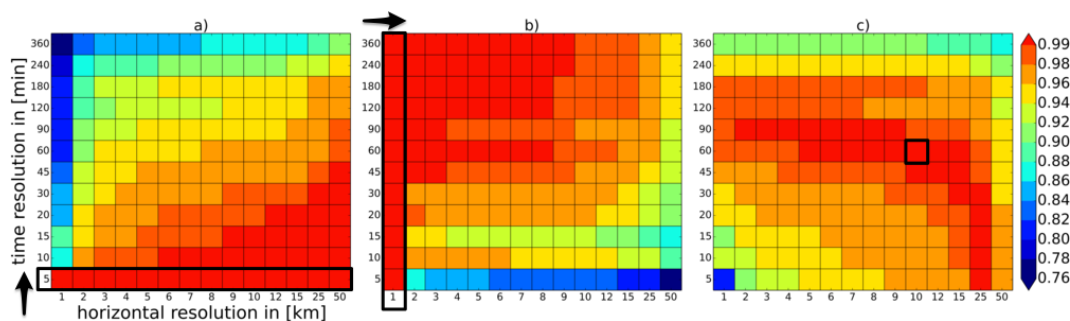


Figure 11. PDF overlap of stratiform precipitation intensity; otherwise similar to Fig. 10.

## 4 Discussion and conclusions

Precipitation is strongly inhomogeneous in time and space. Averaging over a specific temporal or spatial interval therefore transforms the distribution function. The resulting smoothing especially affects the extreme values, as it narrows the distribution function while preserving the mean. In this study, the focus is on how such averaging affects the two synoptically identifiable precipitation types, namely stratiform and convective extreme precipitation events. Convective events are known to produce strong, short-duration and localized precipitation while stratiform events are less bursty and cover larger areas. Using synoptic observations we separate radar-derived high-resolution precipitation intensities conditional on events of either of these two types. Unlike other studies, we here concentrate on the different aggregation behavior of the two precipitation types at different seasons and regions of Germany. Although we have not analyzed this behavior in other regions and climate zones, we expect that the findings will depend on the mean advection velocity and also the orography might have an impact on results.

### 4.1 Space–time dependency of intensity distributions

We found that convective extremes were considerably stronger in the south than in the north of Germany and also showed clear seasonal differences with the highest extremes occurring in summer. Stratiform extremes showed much more moderate differences over seasons and regions.

When aggregating data temporally or spatially, we find much stronger reduction for convective than for stratiform events (about 20 to 30 % higher). These differences are larger than seasonal or regional differences that were observed within one type. This highlights the importance of distinguishing between these two types of events, for example for statistical downscaling exercises. After the type separation, only the convective extremes show clear regional and seasonal differences and only in the area reduction factors. For the convective type, the strongest intensity reductions with

spatial scale were found in southern Germany in summer and the lowest in northern Germany in winter.

### 4.2 Temporal and spatial scales at which shifts occur between dominantly convective and dominantly stratiform extreme events

Depending on the spatial and temporal resolution, different meteorological events will be considered extreme. We point out that this makes it difficult to compare different studies of extremes in which these extremes were defined at different scales. To demonstrate this we present the contribution of convective events to the total, as a function of data aggregation, for the 99th percentile of all precipitation events.

This information is needed to identify which space–time resolutions contain comparable information about the distribution function, including the extremes. It will further help to identify at which resolution and percentile one can expect to obtain information about convective extreme precipitation events. Besides expected seasonal and regional differences with higher contribution of convective events in summer and over southern Germany, we also found a clear dependency on the scale and the threshold used. Over northern Germany, stratiform events contribute to the 99th percentile extremes only at horizontal resolutions coarser than 12 km when the duration interval is kept constant to 5 min. For a higher threshold (99.9th percentile), convective events dominate even more strongly and convective extremes consequently prevail over even larger areas and durations.

### 4.3 Pairs of temporal and spatial resolutions with similar aggregation effects on the extremes

For proper choice of model output resolution, precipitation downscaling as well as bias correction, the relation between the DRFs as compared to ARFs is important. Originating from the radar data resolution of 5 min temporally and 1 km spatially, we produced sequences of aggregation, both in space and time, yielding (i) temporally aggregated intensities for spatial scales held fixed and (ii) spatially aggregated intensity for temporal scales held fixed. Associating the respective aggregation resolution by matching identical pre-

precipitation extremes, we yield pairs of temporal and spatial resolutions, which define a curve.

The results allow us, e.g., to identify pairs ( $\Delta x$ ,  $\Delta t$ ) of spatial and temporal resolutions for which the decrease in extreme precipitation intensities due to temporal aggregation matches that due to horizontal aggregation. In terms of the Taylor hypothesis, the timescales can roughly be viewed as the mean duration needed to advect the precipitation pattern by the width of a grid box (Fig. 6).

For example, if for a given horizontal grid size a larger temporal output interval is used the event will likely be advected further than the size of the grid box, leading to strong duration reduction factors. We find that for state-of-the-art regional climate simulations, performed at a 11 km horizontal resolution, the temporal resolution needed in order to avoid stronger duration than area reduction effects would be approximately 20 to 25 min.

In practice, in regional climate models the temporal output is often lower than the resolution computed here. It should therefore be reconsidered why many regional models do not output at sub-hourly frequency and why often only daily averages are stored.

If a model can resolve some small-scale features, e.g., convective extremes, information can only be preserved by outputting at the appropriate temporal resolution, while information gets lost when using lower temporal resolutions (Fig. 8). High temporal resolution is accessible by most models already (most models have computing time steps  $\sim$  seconds–minutes) but is not routinely output at such short periods. Recording at higher frequency would mainly affect storage space and not simulation run time (assuming efficient I/O handling).

The pairs of corresponding grid sizes and durations define a velocity  $v_{\text{eff}}$ , which can be used to generalize the Taylor hypothesis to the situation where temporal scales change disproportionately compared to spatial scales (self-affinity; Deidda, 2000). For constant  $v_{\text{eff}}$  as function of spatial scale, the Taylor hypothesis would be obeyed. However,  $v_{\text{eff}}$  of convective and stratiform extreme precipitation algebraically decreases with increasing  $\Delta x$  with similar exponents for both precipitation types. The main scaling difference between convective and stratiform events can be described by a constant scaling factor. This scaling factor leads to about 1.75 times higher advection velocities for stratiform than for convective events.

#### 4.4 PDF overlap

Changes caused by temporal aggregation depend on the spatial scale of the data and vice versa. We examine these dependencies by comparing pairs of PDFs derived for different aggregation resolutions using a method developed by Perkins et al. (2007), here defined as PDF overlap.

We find that PDF changes that were observed when decreasing the temporal resolution from 5 min to 2 h at 50 km

horizontal resolution are quantitatively comparable with PDF changes when going from 5 to 30 min at 10 km horizontal resolution or from 5 to 10 min at 2 km horizontal resolution.

Furthermore, we show that the PDF overlap of a certain reference resolution (we chose as an example 60 min, 10 km) compared to all other aggregated resolutions shows a ridge with values close to 1. This ridge ranges from 5 min and 25 km to 120 min at 1 km resolution for convective type events (Fig. 10c) and from 5 min and 25 km to 90 min at 1 km resolution for stratiform events (Fig. 10c). These differences can be explained by the strong area reduction factors found for the convective type. The patterns found in this analysis are very similar to the patterns found in Figs. 3 and 4, highlighting that most of the differences found in the PDF overlap result from changes in the extremes.

**The Supplement related to this article is available online at doi:10.5194/acp-15-5957-2015-supplement.**

*Acknowledgements.* The authors acknowledge the radar data from the German Weather Service (DWD). We further acknowledge the provision of station data from the British Met Office for provision of the Met Office Integrated Data Archive System (MIDAS) for the synoptic codes, retrieved through the British Atmospheric Data Centre (BADC). B. Eggert acknowledges support from Climate Service Center 2.0; P. Berg acknowledges support from SMHI; J. O. Haerter acknowledges support from the Danish National Research Foundation through the Center for Models of Life; and C. Moseley acknowledges support from the project HD(CP)<sup>2</sup>, funded by the German Federal Ministry of Education and Research.

The article processing charges for this open-access publication were covered by a Research Centre of the Helmholtz Association.

Edited by: P. Chuang

#### References

- Arnbjerg-Nielsen, K., Willems, P., Olsson, J., Beecham, S., Pathirana, A., Bülow Gregersen, I., Madsen, H., and Nguyen, V.-T.-V.: Impacts of climate change on rainfall extremes and urban drainage systems: a review, *Water Sci. Technol.*, 68, 16–28, doi:10.2166/wst.2013.251, 2013.
- Attema, J. J., Loriaux, J. M., and Lenderink, G.: Extreme precipitation response to climate perturbations in an atmospheric mesoscale model, *Environ. Res. Lett.*, 9, 014003, doi:10.1088/1748-9326/9/1/014003, 2014.
- Austin, P. M., and Houze Jr., R. A.: Analysis of the structure of precipitation patterns in New England, *J. Appl. Meteorol.*, 11, 926–935, doi:10.1175/1520-0450(1972)011<0926:AOTSOP>2.0.CO;2, 1972.
- Bacchi, B. and Ranzi, R.: On the derivation of the areal reduction factor of storms, *Atmos. Res.*, 42, 123–135, doi:10.1016/0169-8095(95)00058-5, 1996.

- Berg, P., Moseley, C., and Haerter, J. O.: Strong increase in convective precipitation in response to higher temperatures, *Nat. Geosci.*, 6, 181–185, doi:10.1038/ngeo1731, 2013.
- Berndtsson, R. and Niemczynowicz, J.: Spatial and temporal scales in rainfall analysis – Some aspects and future perspectives, *J. Hydrol.*, 100, 293–313, 1988.
- Blöschl, G. and Sivapalan, M.: Scale issues in hydrological modelling: a review, *Hydrol. Process.*, 9, 251–290, doi:10.1002/hyp.3360090305, 1995.
- Collins, M., Knutti, R., Arblaster, J., Dufresne, J.-L., Fichet, T., Friedlingstein, P., Gao, X., Gutowski, W., Johns, T., Krinner, G., Shongwe, M., Tebaldi, C., Weaver, A., and Wehner, M.: Long-term climate change: projections, commitments and irreversibility, in: *Climate Change 2013: the Physical Science Basis, Contribution of Working Group I to the Fifth Assessment Report of the Intergovernmental Panel on Climate Change*, edited by: Stocker, T. F., Qin, D., Plattner, G.-K., Tignor, M., Allen, S. K., Boschung, J., Nauels, A., Xia, Y., Bex, V., and Midgley, P. M., Cambridge University Press, Cambridge, UK and New York, NY, USA, 2013.
- Deidda, R.: Rainfall downscaling in a space-time multifractal framework, *Water Resour. Res.*, 36, 1779–1794, doi:10.1029/2000WR900038, 2000.
- De Toffol, S., Laghari, A. N., and Rauch, W.: Are extreme rainfall intensities more frequent? Analysis of trends in rainfall patterns relevant to urban drainage systems, *Water Sci. Technol.*, 59, 1769–1776, doi:10.2166/wst.2009.182, 2009.
- Haerter, J. O., Eggert, B., Moseley, C., Piani, C., and Berg, P.: Statistical precipitation bias correction of gridded model data using point measurements, *Geophys. Res. Lett.*, 42, 1919–1929, doi:10.1002/2015GL063188, 2015.
- Hartmann, D., Tank, A. K., Rusticucci, M., Alexander, L., Brönnimann, S., Charabi, Y., Dentener, F., Dlugokencky, E., Easterling, D., Kaplan, A., Soden, B., Thorne, P., Wild, M., and Zhai, P.: Observations: atmosphere and surface, in: *Climate Change 2013: the Physical Science Basis, Contribution of Working Group I to the Fifth Assessment Report of the Intergovernmental Panel on Climate Change*, Cambridge University Press, Cambridge, UK and New York, NY, USA, 2013.
- Houze, R. A.: Stratiform precipitation in regions of convection: a meteorological paradox?, *B. Am. Meteorol. Soc.*, 78, 2179–2196, doi:10.1175/1520-0477(1997)078<2179:SPIROC>2.0.CO;2, 1997.
- Houze Jr., R. A., and Hobbs, P. V.: Organization and structure of precipitating cloud systems, *Adv. Geophys.*, 24, 225–315, 1982.
- Kendon, E. J., Roberts, N. M., Fowler, H. J., Roberts, M. J., Chan, S. C., and Senior, C. A.: Heavier summer downpours with climate change revealed by weather forecast resolution model, *Nat. Clim. Change*, 4, 1–7, doi:10.1038/NCLIMATE2258, 2014.
- Khodayar, S., Kalthoff, N., and Scha, G.: The impact of soil moisture variability on seasonal convective precipitation simulations, Part I: Validation, feedbacks, and realistic initialisation, *Meteorol. Z.*, 22, 489–505, doi:10.1127/0941-2948/2013/0403, 2013.
- Kunz, M.: Von Wettersystemen zu Extremereignissen: Gefährdungsanalyse über orografisch strukturiertem Gelände, in: *Verständnis, Vorsorge und Bewältigung von Naturkatastrophen, Abschlussworkshop 2007, Graduiertenkolleg “Naturkatastrophen”, 24/25 July 2007*, edited by: Senitz, S., Universitätsverlag, Karlsruhe, 195–203, 2007.
- Kunz, M., Sander, J., and Kottmeier, C.: Recent trends of thunderstorm and hailstorm frequency and their relation to atmospheric characteristics in southwest Germany, *Int. J. Climatol.*, 29, 2283–2297, doi:10.1002/joc.1865, 2009.
- Lenderink, G. and van Meijgaard, E.: Increase in hourly precipitation extremes beyond expectations from temperature changes, *Nat. Geosci.*, 1, 511–514, doi:10.1038/ngeo262, 2008.
- Marani, M.: On the correlation structure of continuous and discrete point rainfall, *Water Resour. Res.*, 39, 1128, doi:10.1029/2002WR001456, 2003.
- Marani, M.: Non-power-law-scale properties of rainfall in space and time, *Water Resour. Res.*, 41, W08413, doi:10.1029/2004WR003822, 2005.
- Marchi, L., Borga, M., Preciso, E., and Gaume, E.: Characterisation of selected extreme flash floods in Europe and implications for flood risk management, *J. Hydrol.*, 394, 118–133, doi:10.1016/j.jhydrol.2010.07.017, 2010.
- Michele, C. D., Kottegoda, N. T., Rosso, R., and De Michele, C.: The derivation of areal reduction factor of storm rainfall from its scaling properties, *Water Resour. Res.*, 37, 3247–3252, doi:10.1029/2001WR000346, 2001.
- Moseley, C., Berg, P., and Haerter, J. O.: Probing the precipitation life cycle by iterative rain cell tracking, *J. Geophys. Res.-Atmos.*, 118, 13361–13370, doi:10.1002/2013JD020868, 2013.
- Mueller, E. N. and Pfister, A.: Increasing occurrence of high-intensity rainstorm events relevant for the generation of soil erosion in a temperate lowland region in Central Europe, *J. Hydrol.*, 411, 266–278, doi:10.1016/j.jhydrol.2011.10.005, 2011.
- Muller, C. J., O’Gorman, P. A., and Back, L. E.: Intensification of Precipitation Extremes with Warming in a Cloud-Resolving Model, *J. Climate*, 24, 2784–2800, doi:10.1175/2011JCLI3876.1, 2011.
- Onof, C., Northrop, P., Wheeler, H. S., and Isham, V.: Spatiotemporal storm structure and scaling property analysis for modeling, *J. Geophys. Res.*, 101, 26415, doi:10.1029/96JD01378, 1996.
- Perkins, S. E., Pitman, A. J., Holbrook, N. J., and McAneney, J.: Evaluation of the AR4 climate models’ simulated daily maximum temperature, minimum temperature, and precipitation over Australia using probability density functions, *J. Climate*, 20, 4356–4376, doi:10.1175/JCLI4253.1, 2007.
- Piani, C., Haerter, J., and Coppola, E.: Statistical bias correction for daily precipitation in regional climate models over Europe, *Theor. Appl. Climatol.*, 99, 187–192, 2010a.
- Piani, C., Weedon, G., Best, M., Gomes, S., Viterbo, P., Hagemann, S., and Haerter, J.: Statistical bias correction of global simulated daily precipitation and temperature for the application of hydrological models, *J. Hydrol.*, 395, 199–215, 2010b.
- Schertzer, D. and Lovejoy, S.: Physical modeling and analysis of rain and clouds by anisotropic scaling multiplicative processes, *J. Geophys. Res.*, 92, 9693–9714, 1987.
- Sivapalan, M. and Blöschl, G.: Transformation of point rainfall to areal rainfall: intensity-duration-frequency curves, *J. Hydrol.*, 204, 150–167, 1998.
- Smith, J., Bradley, A., and Baeck, M.: The space-time structure of extreme storm rainfall in the southern plains, *J. Appl. Meteorol.*, 33, 1402–1417, doi:10.1175/1520-0450(1994)033<1402:TSSOES>2.0.CO;2, 1994.

- Steiner, M., Smith, J. A., and Uijlenhoet, R.: A microphysical interpretation of radar reflectivity-rain rate relationships, *J. Atmos. Sci.*, 61, 1114–1131, 2004.
- Taylor, G.: The spectrum of turbulence, *P. Roy. Soc. Lond.*, 164, 476–490, 1938.
- Trenberth, K. E.: Conceptual Framework for Changes of Extremes of the Hydrological Cycle with Climate Change, Springer Netherlands, 327–339, doi:10.1007/978-94-015-9265-9\_18, 1999.
- Trenberth, K. E.: Changes in precipitation with climate change, *Clim. Res.*, 47, 123–138, doi:10.3354/cr00953, 2011.
- Trenberth, K. E., Dai, A., Rasmussen, R. M., and Parsons, D. B.: The changing character of precipitation, *B. Am. Meteorol. Soc.*, 84, 1205–1217, doi:10.1175/BAMS-84-9-1205, 2003.
- Waymire, E., Gupta, V. K., and Rodriguez-Iturbe, I.: A spectral theory of rainfall intensity at the meso- $\beta$  scale, *Water Resour. Res.*, 20, 1453–1465, doi:10.1029/WR020i010p01453, 1984.
- Westra, S., Fowler, H. J., Evans, J. P., Alexander, L. V., Berg, P., Johnson, F., Kendon, E. J., Lenderink, G., and Roberts, N. M.: Future changes to the intensity and frequency of short-duration extreme rainfall, *Rev. Geophys.*, 52, 2014RG000464, doi:10.1002/2014RG000464, 2014.
- Willems, P., Arnbjerg-Nielsen, K., Olsson, J., and Nguyen, V.: Climate change impact assessment on urban rainfall extremes and urban drainage: methods and shortcomings, *Atmos. Res.*, 103, 106–118, doi:10.1016/j.atmosres.2011.04.003, 2012.
- Wood, A. W., Leung, L. R., Sridhar, V., and Lettenmaier, D.: Hydrologic implications of dynamical and statistical approaches to downscaling climate model outputs, *Climatic Change*, 62, 189–216, 2004.
- Zawadzki, I.: Statistical properties of precipitation patterns, *J. Appl. Meteorol.*, 12, 459–472, doi:10.1175/1520-0450(1973)012<0459:SPOPP>2.0.CO;2, 1973.